

Theoretical Modeling of Enzyme Reactions: The Thermodynamics of Formation of Compound 0 in Horseradish Peroxidase

Costantino Zazza,^{†,‡} Andrea Amadei,^{*,§} Amedeo Palma,^{*,||} Nico Sanna,[†] Simone Tatoli,^{†,⊥} and Massimiliano Aschi[‡]

Consorzio Interuniversitario per le Applicazioni di Supercalcolo per Università e Ricerca (CASPUR), Via dei Tizii 6b, 00185 Roma, Italy, Dipartimento di Chimica, Ingegneria Chimica e Materiali Università di L'Aquila, via Vetoio 67100, L'Aquila, Italy, Dipartimento di Scienze e Tecnologie Chimiche, Università di Roma Tor Vergata, Via della Ricerca Scientifica 1 I-00133, Roma, Italy, Istituto per lo Studio dei Materiali Nanostrutturati, CNR-ISMN, Via Salaria km 29.3, Sez. Montelibretti, Monterotondo S. (RM), Italy, and Dipartimento di Chimica, Università di Roma "La Sapienza", P.le A. Moro 5, 00185, Roma, Italy

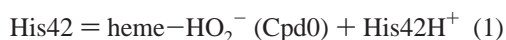
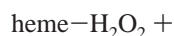
Received: September 17, 2007; In Final Form: December 21, 2007

In this paper, by using the perturbed matrix method (PMM) in combination with basic statistical mechanical relations both based on nanosecond time-scale molecular dynamics (MD) simulations, we quantitatively address the thermodynamics of compound 0 (Cpd 0) formation in horseradish peroxidase (HRP) enzyme. Our results, in the same trend of low-temperature experimental data, obtained in cryoenzymology studies indicate that such a reaction can be described essentially as a stepwise spontaneous process: a first step mechanically constrained, strongly exothermic proton transfer from the heme–H₂O₂ complex to the conserved His42, followed by a solvent–protein relaxation involving a large entropy increase. Critical evaluation of PMM/MD data also reveals the crucial role played by specific residues in the reaction pocket and, more in general, by the conformational fluctuations of the overall environment in physiological conditions.

1. Introduction

Horseradish peroxidase (HRP) is a heme-containing enzyme that catalyzes a variety of organic and inorganic substrates utilizing hydrogen peroxide (H₂O₂). The very early stages of the catalytic process, following the formation of the heme–iron(III) complex with H₂O₂ (heme–H₂O₂), were first described in the 1980s by Poulos and Kraut.¹ These authors proposed a stepwise acid–base process, essentially involving heme–H₂O₂ and the highly conserved His42 and Arg38,² characterized by the formation of two key intermediates, that is, compound 0 (Cpd0) and compound I (CpdI), according to the simplified scheme reported in Figure 1.

Important confirmations of the above mechanism, which nowadays is largely accepted, were provided by experimental evidence of the existence of the intermediates Cpd0 and CpdI.^{3–6} Further experimental studies^{7,8} have also indicated that the first step of the above process, that is, formation of Cpd0 according to eq 1



although strongly unfavorable in aqueous solution,⁹ is a spontaneous and very fast reaction within the protein framework even at low temperature.

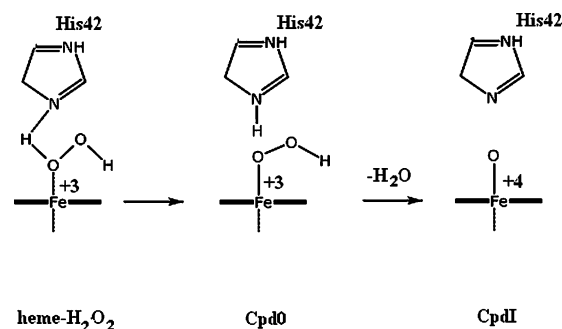


Figure 1. Schematic view of the formation of compound I according to the Poulos–Kraut mechanism. Note that the sixth (axial) iron coordination is occupied by His170 residue not shown for the sake of clarity.

It, therefore, was extremely appealing, in particular for theoreticians, to understand the crucial role of the biological (protein and solvent) environment on the formation of Cpd0. In this respect, recent computational studies carried out on simplified models in vacuo^{10–13} or using quantum mechanics molecular mechanics (QM/MM) schemes¹⁴ have provided important insight into the intrinsic electronic complexity of reaction 1, witnessing the strong difficulties in terms of computational/theoretical modeling of the reaction process, which could also involve different magnetic states.^{13,14b}

It is in general widely accepted that reliable modeling of chemical reactions taking place in an enzyme environment, and more in general in complex systems, does represent nowadays one of the challenges of theoretical physical chemistry.^{15,16} The primary difficulty is represented by the necessity of maintaining the electronic detail of the covalent (chemical) transition, within a configurationally complex atomistic environment, which is

* Corresponding authors. E-mail: andrea.amadei@uniroma2.it; amedeo.palma@ismn.cnr.it.

[†] CASPUR.

[‡] Ingegneria Chimica e Materiali Università di L'Aquila.

[§] Università di Roma Tor Vergata.

^{||} Istituto per lo Studio dei Materiali Nanostrutturati, CNR-ISMN.

[⊥] Università di Roma "La Sapienza".

peculiar, for example, in bio-macromolecular systems. Recently, we have proposed a theoretical—computational approach, the perturbed matrix method (PMM)^{17,18} whose primary goal is the inclusion of the electronic degrees of freedom within a sufficiently exhaustive configurational sampling of the overall atomistic environment typically obtained using either force-field-based molecular dynamics (MD) or Monte Carlo simulations. Encouraging results provided by PMM for different systems^{19–22} have induced us to address reaction 1 with the same approach. Because of the high complexity of the problem, we will limit our attention on the thermodynamics of the formation of Cpd0 trying to underline as much as possible the effects of the presence of the enzyme and the solvent. The underlying perspective of PMM, in line with basically all QM/MM procedures, relies on the pre-definition of a portion of the system to be explicitly treated at the electronic level, that is, the quantum centre (QC) whose critical definition is determined from the results of MD simulations. The first part of the present study is in fact devoted to the MD-based strategy for defining and optimizing the QC structure. In the final part of the paper, the full thermodynamics associated with reaction 1 will be outlined.

2. Computational Details

2.1. Molecular Dynamics Simulations of Peroxy Complex and Compound 0. The primary condition, necessary for PMM calculations, is the production of the MD trajectories of the initial and final states of reaction 1. Simulations were initiated using, as starting coordinates, HRP monomer extracted from the crystal structure of recombinant peroxidase (pdb code: 1ATJ). In the first simulated system, hereafter termed as peroxy complex, one H₂O₂ molecule was used for saturating the sixth coordination of iron to form heme—H₂O₂. In the second simulated system, hereafter termed as Cpd0, we used exactly the same starting coordinates of the first simulation with one proton shifted from heme—H₂O₂ to His42. Note that in the present study, focused on the thermodynamics of the reaction, we will not explicitly have to deal with the actual mechanism of the proton transfer. We wish to further point out that the terms peroxy complex and Cpd0 will be hereafter indicating the two overall simulated systems. Structural Ca²⁺ ions were also included in the system because of their documented importance in maintaining the structural integrity of heme.²³ The solute (HRP monomer with heme—H₂O or heme—HOO[−]) was put at the center of a rectangular box (7.4484 × 8.7176 × 6.9747 nm³) filled with single point charge²⁴ (SPC) water molecules at a density of 1000 kg/m³ (13 371 molecules) and one chloride ion for ensuring electrical neutrality. A standard protocol was adopted for initiating the simulations: following a mechanical solute optimization and subsequent solvent relaxation, the system was gradually heated from 50 to 300 K using short (20 ps) MD simulations. The trajectories were then propagated for 20 ns in a NVT ensemble using an integration step of 2.0 fs with the roto-translational constraint²⁵ applied to the solute. The temperature was kept constant by the isokinetic temperature coupling,²⁶ and all bond lengths were constrained using LINCS algorithm.²⁷ Long-range electrostatics was computed by the particle mesh Ewald (PME) method,²⁸ with 34 wave vectors in each dimension and a fourth-order cubic interpolation. A cutoff of 1.1 nm was used, and pair list was updated every five integration steps. Gromos96 force field²⁹ parameters were adopted for the protein and heme groups, whereas for H₂O₂ and iron the point charges (0.8 au for iron, −0.3 au for oxygens, and +0.3 au for hydrogens) were recalculated by standard fitting procedure³⁰ using density

functional theory³¹ calculations with Becke's three parameters exchange and Lee, Yang, and Parr correlation functionals (B3LYP) with the following atomic basis sets: (i) for iron we used LANL2DZ effective core potential for the inner electrons and a double- ζ Gaussian basis set of (5S,5P,5D)/[3S,3P,2D] quality for valence electrons;³² (ii) for nitrogen and oxygen we used a standard 6-311G(d)³³ Gaussian basis set; (iii) for carbon and hydrogen the 3-21G Gaussian basis set was adopted. This level of theory will be hereafter termed as B3LYP/BS1. Note that for iron—oxygen, oxygen—oxygen (peroxide), and oxygen—hydrogen (peroxide) we used 0.2307, 0.1479, and 0.1 nm bond lengths, respectively, with force constants of 6.05×10^5 , 8.05×10^5 , and $374\,468 \text{ kJ mol}^{-1}\text{nm}^{-2}$. Essential dynamics (ED) analysis³⁴ of the trajectories of atomic coordinates was used to characterize conformational changes. This method consists of building the covariance matrix of the atomic positional fluctuations obtained from MD simulations. After its diagonalization, an orthonormal set of eigenvectors defines a new set of generalized coordinates along which the fluctuations occur. The eigenvectors with the largest eigenvalues allow us to define the essential subspace where to search for the relevant conformational transitions. All of the simulations were carried out using the Gromacs software, version 3.0.3³⁵ modified to include the roto-translational constraint and isokinetic temperature coupling.

2.2. Perturbed Matrix Method Calculations. Details of PMM calculations are widely illustrated in our previous studies, which we invite the interested reader to refer to.^{17–22,36} After the critical definition of the QC, B3LYP/BS1 calculations were carried out on the corresponding relaxed geometries (see following sections) for obtaining ground-state energies and related properties. Note that, following the indications of previous studies,^{13,14} we limited our attention to the doublet magnetic state. Subsequently, the first eight unperturbed excited electronic states were obtained on the same geometries using configuration interaction calculations with single excitations (CIS/BS1), driven by time-dependent DFT calculations. Although in general this level of theory does not provide a fully correct description of electronic excited states, in the case of the heme group it already proved to represent a good compromise between computational costs and chemical accuracy.^{36a}

These quantum chemical calculations, carried out on each chemical species describing reaction 1 (see below), provided the nine-dimensional *unperturbed* basis set to be used for constructing and diagonalizing, at each step of MD simulation, the perturbed electronic Hamiltonian according to PMM procedure. As a result we obtain, along the overall trajectory, a set of eigenvalues (ϵ) and eigenvectors to be used for calculating the free energy, internal energy, and entropy associated with reaction 1 according to the approach outlined in the Subsection 3.4 and in the Appendix. All quantum chemical calculations were carried out using the Gaussian03 package.³⁷

3. Results and Discussion

3.1. Mechanical Properties of HRP Protein Framework. Both simulations, propagated for 20 ns and excluding an initial drift, show a rather low C-alpha root-mean-square deviation (rmsd), with respect to the initial (crystal) structure, equal to 0.19 ± 0.02 and 0.16 ± 0.02 nm for Cpd0 and peroxy complex, respectively. These values are in line with previous long-scale simulations carried out on native HRP and with HRP—anthraquinone 2-carboxylic acid complex.³⁸ Consistently, the C-alpha root-mean-square fluctuation (RMSF), calculated for both systems and reported in Figure 2, indicates a rather rigid protein framework.

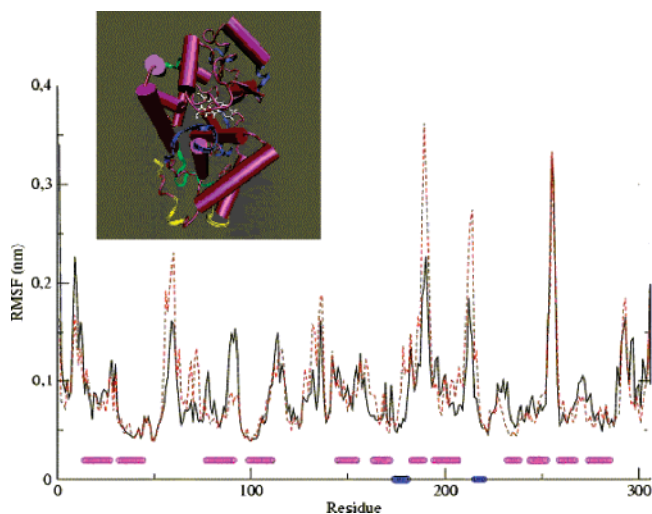


Figure 2. C-alpha RMSF of peroxy-complex (red-dotted) and Cpd0 (black) simulations. In the same figure, we also report in magenta and blue, along the abscissa, α -helix and β -strand crystallographic regions (1ATJ). In the inset, we have reported the pictorial representation of the regions whose fluctuations undergo relevant decrease (lower than 0.05 nm, indicated in blue) or increase (larger than 0.05 nm, indicated in yellow) upon chemical transition from peroxy complex to Cpd0. Regions whose fluctuations remains essentially unaltered are indicated in green.

High fluctuations are concentrated, as usual, in non-structured solvent exposed regions while alpha-helices and beta-strands, indicated in Figure 2 in magenta and blue, respectively, are only marginally involved. Interestingly, RMSFs are poorly superimposable, with differences schematically shown in the inset of Figure 2, clearly suggesting a slight transition in the fluctuation pattern upon heme-H₂O₂/His42 proton transfer. Consistently, the eigenvalues of the C-alpha covariance matrix reported in Figure 3, clearly show a decrease of fluctuation when passing from peroxy complex to Cpd0.

The above simulations represent the basis for the detailed study of reaction 1 provided we may define the QC. The definition of QC is essentially driven by the problem at hand. Hence, in the present case a minimum definition should include the conjugated acid-base pair of reaction 1, that is, heme-H₂O₂ and His42. The problem is to critically evaluate what additional residues/solvent molecules, if any, should be added. It must be always reminded that for providing a good description of the unperturbed electronic states and for allowing a straightforward application of PMM¹⁸ QC must be relatively low-sized and possibly rigid or semirigid in the simulated ensemble. In some cases, it is possible to define the QC before setting the MD simulation, somewhat simplifying the problem.³⁶ In the present study, such a pre-definition would severely affect the final result; for this reason, we carefully selected the QC region on the basis of the above considerations by MD analyses described in the following subsections.

3.2. Mechanical Properties of the Reaction Pocket and Definition of the Quantum Centre. Previous observations have clearly indicated that reaction 1 induces unpredictable variations in the overall system consisting of the protein framework, heme-H₂O₂ complex, and even the solvent. The definition itself of *reaction pocket* (RP) is therefore somewhat arbitrary. Nevertheless, we can try to enucleate from the entire system an atomistic subspace, which, based on previous literature or because of their spatial vicinity to the *breaking covalent bond*, may represent the most influential mechanical “reaction guideline”. On this basis, we have pre-defined, within the peroxy-complex

simulation, as reactant reaction pocket (R-RP) the cluster formed by the heme-H₂O₂ complex and the closest residues, namely, His42, Arg38, Pro139, and the His170 bound to iron, as shown in Figure 4.

Using the same arguments, we therefore defined as product reaction pocket (P-RP) the same R-RP system showing the heme-HOO⁻ and His42H⁺ conjugated pair in the Cpd0 simulation. RMSFs, evaluated for R-RP along the peroxy-complex trajectory, and for P-RP along Cpd0 trajectory, are reported in Figure 5. In the case of R-RP (panel A of Figure 5), we find a very rigid structure with the only, already documented^{36a} exception of the heme side chains, that is, propionate groups.

The situation appears rather modified as far as P-RP is concerned (panel B of the same figure.) In particular, a drastic increase of fluctuation is observed in correspondence of both the His42H⁺ and His170 side chain. According to such analysis both R-RP and P-RP, with the exception of heme propionates, His42H⁺, and His170 side chains, appear as a rather rigid structures in principle suitable for the definition of the QC. Unfortunately, such a choice would prevent whatever meaningful quantum chemical evaluation of the related unperturbed electronic states because of its high dimension. Hence, a further reduction is necessary. For this purpose, we evaluated the equilibrium distances of the different residues with respect to the heme-H₂O₂ moiety by calculating the binding free energy (with respect to the related free-energy minimum) as a function of the distance **R** between each residue of R-RP (and P-RP) and the proximal H₂O₂ proton (the proton bound to the oxygen atom connected to iron, see Figure 1) using the standard equation

$$\Delta A_i(R) = -k_B T \ln \frac{\rho_i(R)}{\rho_i(R^*)} \quad (2)$$

In this equation, $\rho_i(R)$ represents the probability density of finding the *i*th residue at a generic distance *R* from the reference (see below), *R*^{*} is the most probable value of *R* and, consequently, may be defined as the equilibrium distance. This analysis was carried out between each residue of the reaction pocket and the proximal H₂O₂ proton.

According to our results, depicted in Figure 6, Arg38 lies in close and stable contact with respect to water peroxide (*R*^{*} at about 0.19 nm). Alternatively for His42, acting as a base in reaction 1, a larger distance is found (*R*^{*} at about 0.35 nm) resembling the crystal structure. Finally Pro139, found at a distance comparable to that of His42, shows a very broad free-energy profile.

The same analysis, repeated for P-RP with respect to the deprotonated oxygen atom of water peroxide, and reported in Figure 7, does not show any significant variations for Arg38. A rather unaltered situation is found for Pro139, which interestingly shows two minima (see below). In line with the previous RMSF analysis, His42H⁺ turns out to enhance its mobility drastically.

The above results suggest that the Arg38 residue is rigid and very close to water peroxide while Pro139 is rather distant from the acid-base conjugated pair and can be excluded by the definition of the QC. Thus, we may reduce the QC definition including the two reaction partners, that is, heme-H₂O₂ complex and His42 (becoming heme-HOO⁻ and His42H⁺ in Cpd0), Arg38, and His170. In order to further reduce the QC dimensionality, we finally defined chemical groups mimicking the actual residues, that is, imidazole rings for histidines and HC-(NH₂)₃⁺ moiety for arginine, including their remaining parts in the perturbing environment.^{14b}

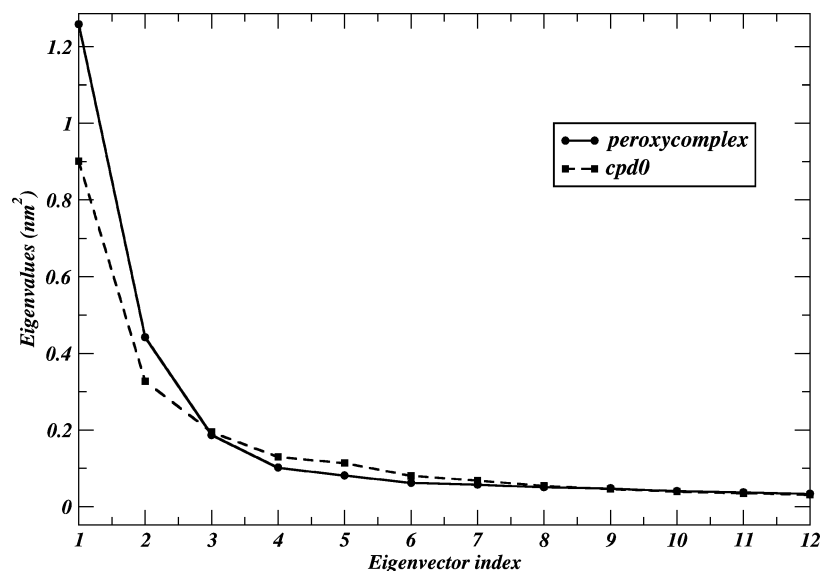


Figure 3. Eigenvalues spectrum of the C-alpha covariance matrix for the two simulated systems.

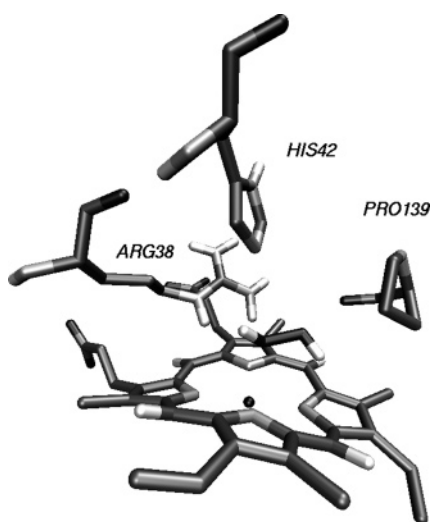
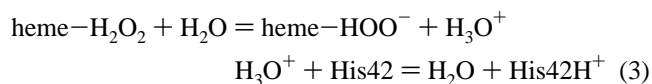


Figure 4. Schematic view of reaction pocket. Note that for the sake of clarity we omitted the bound His170.

There is, at this point, an additional aspect to be addressed for a definitive outline of QC: the plausible presence of water molecules in the reaction mechanism. Recent computational studies¹⁴ have suggested the key role of a water molecule acting as a proton shuttle according to scheme 3



For assessing the validity of the above hypothesis, which would obviously imply the inclusion of one water molecule in the definition of the QC, it is first important to ascertain the actual degree of hydration of R-RP. For this purpose, we constructed an orthogonal reference frame, centered on the H₂O₂ distal proton and defined via one nitrogen atom bound to iron and the iron itself, as depicted in Figure 8.

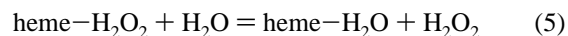
We then defined $\rho(R, \Phi, \Theta)$ as the probability density of finding, along the simulation, one water molecule at the spherical coordinates R, Φ , and Θ within the above reference frame. The analysis has been carried out up to 1.0 nm from the acidic

proton. Defining as $\rho(R^*, \Phi^*, \Theta^*)$ the probability density at the maximum, we may calculate the reversible work for moving one water molecule from R^*, Φ^*, Θ^* to whatever R, Φ , and Θ using the standard relation.

$$\Delta A(R, \Phi, \Theta) = -kT \ln \frac{\rho(R, \Phi, \Theta)}{\rho(R^*, \Phi^*, \Theta^*)} \quad (4)$$

The resulting picture, schematically shown in Figure 9, shows a total absence of water in the vicinity of water peroxide and His42, that is, the conjugated acid–base pair, indicating the presence of a large barrier of free energy protecting the prosthetic center. Water molecules were only found, with high probability (white molecules in Figure 9), close to Arg38 and His170. Other highly hydrated zones (in dark gray in the same figure) were found at larger distances.

The presence of Arg38 seems to prevent the entrance of water molecules providing a highly hydrophobic character to R-RP. Note that the same analysis, carried out for P-RP in the Cpd0 simulation, produced essentially the same picture. Our finding may be indirectly related to experimental evidence showing a decrease of enzyme efficiency upon Arg38Leu point mutation.³⁹ In light of our analysis, it can be inferred that the Arg38 removal plausibly increases water concentration within R-RP producing heme–H₂O₂ complex depletion through mass action on equilibrium 5



In conclusion, the direct role of water molecules in reaction 1, at least within the presently employed force field, can be ruled out. In light of the above analyses, we can definitely consider as QCs, mimicking the two limiting chemical states of reaction 1, the relatively rigid clusters His170–heme–H₂O₂–His42–Arg38 and His170–heme–HOO[−]–His42H⁺–Arg38 for peroxy complex and Cpd0, respectively. As a final step, for the application of PMM we need to extract the actual QC geometries to be used in quantum-chemical calculations. Let us reconsider the RP fluctuations by limiting our attention on the QC subsystem. For this purpose, we extracted the trajectories of the previously defined QCs from peroxy-complex and Cpd0 trajectories. These two filtered trajectories were first concatenated, then an all-atom covariance matrix was constructed and

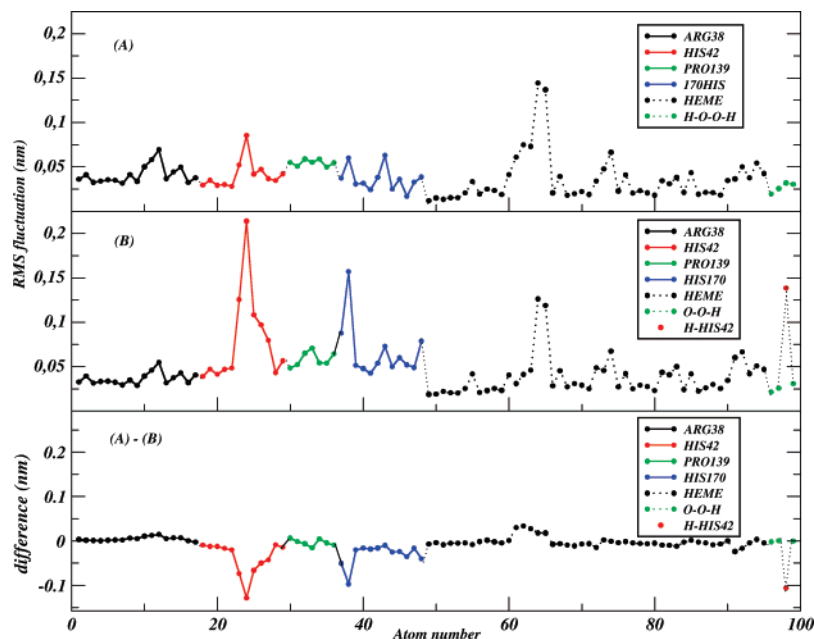


Figure 5. Root-mean-square fluctuation (RMSF) of reaction pocket (see text for the definition) along peroxy-complex (panel A) and Cpd0 (panel B) trajectories. Third panel (A – B) represents the RMSF difference between A and B.

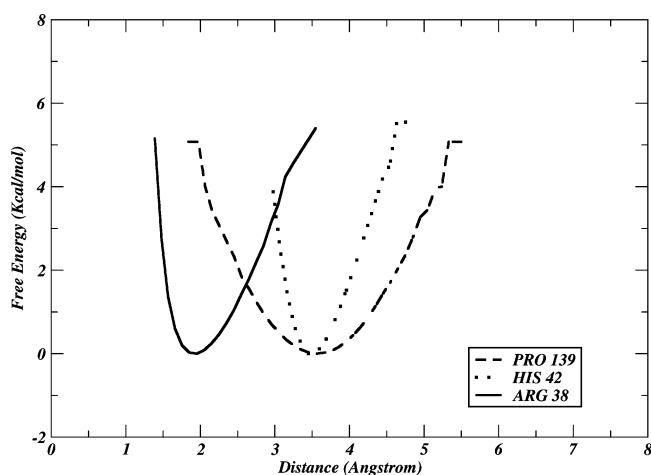


Figure 6. Relative binding free-energy curves (with respect their minimum value taken as reference condition) between indicated residue and proximal H₂O₂ proton. We report interatomic distances between the proximal H₂O₂ proton and the oxygen atom of Pro-139, the nitrogen atom of His42, and the closest NH₂ group of Arg38.

diagonalized. The resulting spectrum of eigenvalues shows the presence of two conformationally relevant (high amplitude) eigenvectors, which almost entirely describe the reactant–product transition. The trajectories were then projected on the plane defined by the above essential eigenvectors, and the result is reported in Figure 10.

We first observe that chemical transformation in the QCs corresponds to a sharp transition in the configurational space, that is, from right to left. Moreover, although the QC of the peroxy complex is confined within the right-side basin of the essential plane (hereafter termed as R), the QC of Cpd0 is split in two conformational basins, hereafter termed as P₁ and P₂. A deep inspection⁴⁰ of the three configurational basins allowed us to extract the R, P₁, and P₂ representative structures reported in the same figure corresponding to each basin. It is interesting to observe that the transition from P₁ to P₂ conformational basins is practically dominated by His42H⁺ torsion (which already

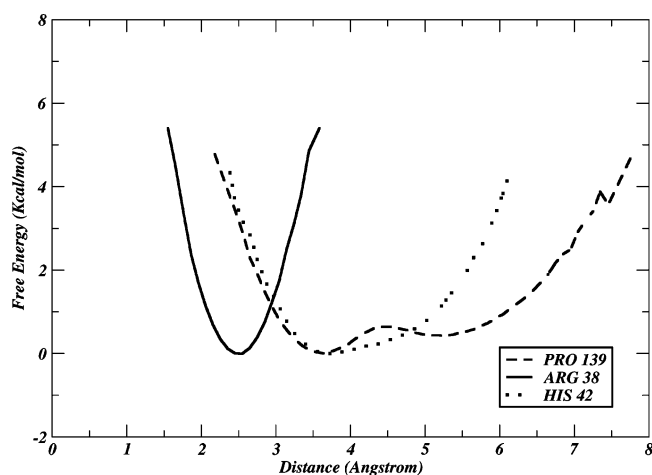


Figure 7. Binding free-energy curves (with respect their minimum value taken as reference condition) in Cpd0, between indicated residue and deprotonated oxygen atom of H₂O₂. We report interatomic distances between the deprotonated H₂O₂ oxygen and the proton bound to His42H⁺, the oxygen atom of Pro-139, and the closest NH₂ group of Arg38.

showed high fluctuation in Cpd0 simulation, see also Figure 6). Also, Pro139 (not included in the figure) shows essentially a similar pattern qualitatively explaining the double-well free-energy minimum observed in Figure 7.

3.3. PMM Calculations and Thermodynamics of Formation of Cpd0. We are now in the position of carrying out PMM calculations and addressing the thermodynamics of reaction 1 according to MD and PMM results. First of all, because of the total absence of overlap of R, P₁, and P₂ basins, that is, between reactant and products onto the essential plane, we assume the reaction to occur according to the following steps:



In the first step (6a), while the system is confined within the peroxy complex ensemble, the proton moves from heme–H₂O₂

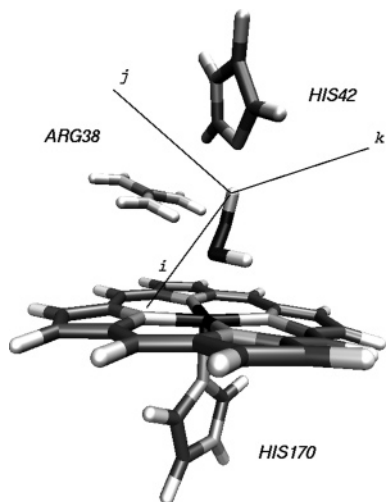


Figure 8. Rigid QC structure for spherical coordinate definition. The depicted unit vectors define the spherical coordinates; R is the distance (norm of \mathbf{R} vector) of water molecule (oxygen atom) with respect the origin, Φ is the angle between the projection of R onto the ij plane and the i unit vector, and Θ is the projection of R on k unit vector.

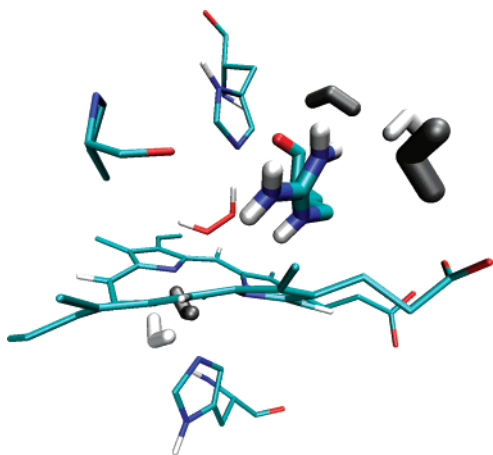


Figure 9. Occurrence of water molecules in the reaction pocket. The reference position (R^* , Φ^* , Θ^*) corresponds to the water molecule bound to His170. In dark-gray, we indicate lower probability positions (almost 14 kJ/mol higher than R^* , Φ^* , Θ^*) found for peroxy-complex simulation.

to His42. Such a process, hereafter indicated as “vertical” proton transfer, occurs with the QC conformation mechanically hindered. Note that such a possibility has already been investigated and proposed by other recent studies.¹⁴ Therefore, P_R is a reaction intermediate state where only the proton is moved to the product covalent condition. In the second step (6b), the system, with the covalent framework already resembling the product relaxes to the Cpd0 ensemble characterized by the $P_1 \rightleftharpoons P_2$ conformational equilibrium. In order to evaluate the (Helmholtz) reaction free energy associated with step 6a ($\Delta A_{R \rightarrow P_R}$), we used eq 7¹⁸

$$\Delta A_{R \rightarrow P_R} = -k_B T \ln \langle \exp[-\beta(\epsilon_{P_R} - \epsilon_R)] \rangle_R \quad (7)$$

In the above equation, ϵ_i represents the perturbed ground-state electronic energy of the i th chemical state (e.g., the reactant or the product) directly evaluated, within certain approximations,¹⁸ by diagonalizing at each MD frame the perturbed Hamiltonian matrix according to the PMM procedure using as basis set the

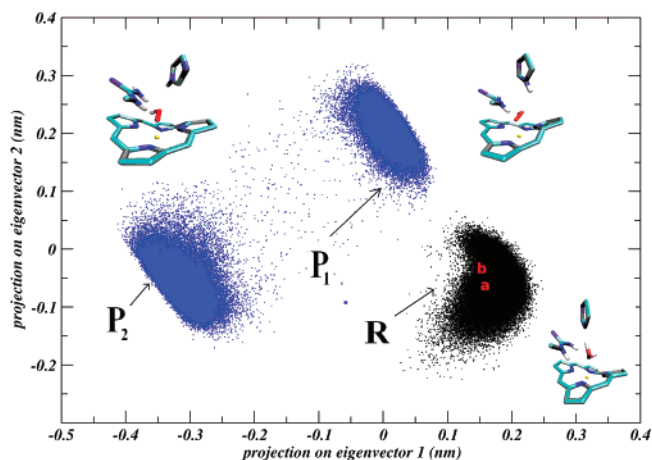


Figure 10. Projection of the all-atom QC trajectories of peroxy complex and Cpd0 onto the essential plane from diagonalization of the covariance matrix obtained by concatenated peroxy-complex and Cpd0 QC trajectories. In the same figure, representative structures of R, P_1 , and P_2 basins are also indicated. The letters a and b in the R basin indicate the relaxed structures used for evaluating unperturbed states of step 6a (see below).

unperturbed states evaluated in correspondence of the representative structures of R and P_R . Note that eq 7, as utilized in the present work, may in principle only provide the free-energy change between two QC rigid structures, that is, the representative structures for the chemical transition. However, assuming for the semirigid QC in each free-energy basin, similar configurational fluctuations, such a free-energy change is virtually identical to the free-energy difference between two different basins, now also including local QC structural fluctuations. Such an approximation will also be used for all of the evaluated free-energy and internal-energy variations between the different basins. In order to avoid spurious effects on the quality of the wavefunction, we relaxed the free-energy basin representative structure slightly in vacuo using B3LYP/B1 calculations. Subsequently, the first eight doublet excited states were evaluated at the CIS/B1 level of theory. The same procedure was adopted for both R and P_R structures. The latter one was obtained just by shifting the proton from heme-H₂O₂ to His42. Note that in both cases B3LYP/B1 geometry relaxations in vacuo (up to a gradient of about 0.01 au), necessary for avoiding spurious effects on the quality of the unperturbed wavefunction, were carried out keeping the structures within R basin and correspond to points a and b of Figure 10 and the related geometries are reported in Figure 11.

Note also that the average in eq 7 is evaluated within the peroxy-complex trajectory, that is, the R ensemble. For calculating the free energy associated with the $P_R \rightarrow P_1$ transition, similar to the previous case, we used eq 8

$$\Delta A_{P_1 \rightarrow P_R} = -k_B T \ln \langle \exp[-\beta(\epsilon_{P_R} - \epsilon_{P_1})] \rangle_{P_1} \quad (8)$$

in which the average was calculated within the P_1 basin and the perturbed ground state energies were obtained using the unperturbed states of P_1 and P_R representative structures.

The free energy associated with the transition from P_1 to P_2 was evaluated by the standard relation

$$\Delta A_{P_1 \rightarrow P_2} = -k_B T \ln \chi_P \quad (9)$$

in which χ_P is the probability ratio of the P_2 and P_1 basins. Using the results from the above relationships, we can finally evaluate

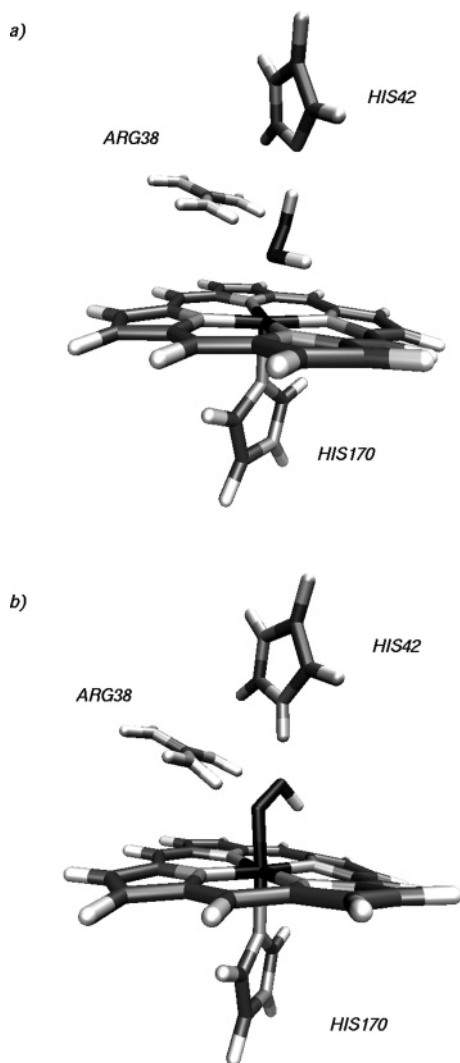


Figure 11. Pictorial representation of R and P_R representative structures (see points a and b in the R basin of Figure 10) used in the PMM calculations for step 6a.

the actual reaction free energy, that is, related to the overall reaction 1, according to eq 10

$$\Delta A_{R \rightarrow P} = \Delta A_{R \rightarrow P_1} - k_B T \ln [1 + \exp(-\beta \Delta A_{P_1 \rightarrow P_2})] \quad (10)$$

where $\Delta A_{R \rightarrow P_1} = \Delta A_{R \rightarrow P_R} - \Delta A_{P_1 \rightarrow P_R}$. The internal energy change associated with step 6a, $\Delta U_{R \rightarrow P_R}$, was then calculated using relation 11 whose derivation is shown in the Appendix;

$$\Delta U_{R \rightarrow P_R} \approx \langle \Delta \epsilon_{R \rightarrow P_R} \exp[-\beta(\Delta \epsilon_{R \rightarrow P_R} - \Delta A_{R \rightarrow P_R})] \rangle_R \quad (11)$$

in this equation, obtained by averaging in the peroxy-complex ensemble, that is, R basin, $\Delta \epsilon_{R \rightarrow P_R}$ stands for the perturbed electronic energy change associated with the 6a transition, evaluated by means of PMM. Similarly, the internal energy change associated with the $P_1 \rightarrow P_R$ step was also calculated using eq 12

$$\Delta U_{P_1 \rightarrow P_R} \approx \langle \Delta \epsilon_{P_1 \rightarrow P_R} \exp[-\beta(\Delta \epsilon_{P_1 \rightarrow P_R} - \Delta A_{P_1 \rightarrow P_R})] \rangle_{P_1} \quad (12)$$

where, obviously, the perturbed electronic energy $\Delta \epsilon_{P_1 \rightarrow P_R}$ concerns the step $P_1 \rightarrow P_R$. The internal energy associated with the step $P_1 \rightarrow P_2$ ($\Delta U_{P_1 \rightarrow P_2}$) was obtained, from Cpd0 simulation, using the average energies of the two product basins. From the last expressions, we may readily obtain (after some algebra)

TABLE 1: Thermodynamics of Reaction 1^a

reaction	$\Delta \epsilon^\circ$ (kJ/mol)	ΔA (kJ/mol)	ΔU (kJ/mol)	ΔS (J/mol/K)
$R \rightarrow P_R$	-22	-61 (-44)	-72 (-52)	-37 (-27)
$P_1 \rightarrow P_R$	13	20	12	-26
$P_1 \rightarrow P_2$		-0.7	35	119
reaction 1		-83	-64	63

^a From left to right: unperturbed ground-state B3LYP/BS1 reaction energy, MD/PMM reaction free energy, internal energy, and entropy. In parentheses we report, for reaction step 6a, the corresponding MD/PMM values as evaluated by applying PMM without including QC-water interaction.

the internal energy change for the whole reaction 1

$$\Delta U_{R \rightarrow P} = \Delta U_{R \rightarrow P_1} + \frac{\chi_P}{1 + \chi_P} \Delta U_{P_1 \rightarrow P_2} \quad (13)$$

with $\Delta U_{R \rightarrow P_1} = \Delta U_{R \rightarrow P_R} - \Delta U_{P_1 \rightarrow P_R}$.

Finally, using the reaction free energy and internal energy variations, we may easily evaluate the related entropy change of each step as well as for the whole reaction by the familiar expression

$$\Delta S = \frac{\Delta U - \Delta A}{T} \quad (14)$$

According to our results, reported in Table 1, reaction 1 reveals as a strongly exothermic and spontaneous process at 300 K associated with a sharp entropy increase largely determined by the P_2 conformational state. Interestingly, step 6a is essentially responsible for the large internal energy decrease, and the active site-solvent interaction plays an important role, as clearly indicated by the relatively large internal and free-energy variations obtained by applying PMM without the perturbation of the solvent (numbers in parenthesis in Table 1).

Subsequent entropy stabilization arises from protein and solvent relaxation upon proton transfer ($P_R \rightarrow P_1 + P_2$). Finally, $P_1 \rightleftharpoons P_2$ conformational equilibrium provides an interesting thermodynamic characterization of the two conformations: the P_1 conformation, showing His42H⁺ tightly interacting with HOO⁻, is characterized by lower internal energy and entropy; P_2 conformation, where His42H⁺ is relatively free to move with reduced potential energy fluctuations, is associated with higher energy and entropy values. Unfortunately, we could not find in the literature experimental data on the reaction thermodynamics in the usual biochemical conditions as the ones utilized in our MD simulations. The only available data on such a reaction⁷ were obtained in rather different conditions, -26.0 °C in 50% v/v methanol/buffer solution, hence making difficult any comparison with our calculations. However, the experimentally observed free-energy decrease driven by a large entropy increase is in line with our results. The enthalpy increase observed experimentally, in contrast with our energy decrease, might be explained by the strongly reduced solvent QC dipole interaction as a result of the water/methanol mixture. In fact, inspection of the unperturbed QC electric dipoles of representative structures of R (11.6 D), P_R (17.7 D), and P_1 (22.2 D) basins shows a strong increase of polarity accompanying both the vertical proton transfer, that is, step 6a, and the overall reaction 1, largely providing the internal energy decrease of P_1 and P_2 with respect to R as resulting mainly from the increased active site-water interaction (see Table 1).

Conclusions

MD simulations and PMM calculations were used for studying the thermodynamics of heme-H₂O₂/His42 proton transfer during Cpd0 formation in HRP enzyme. MD simulation data pinpoint the crucial role of highly conserved Arg38 in the reaction, providing a mechanical barrier to water molecules' entrance into the reaction pocket. Such a result seems to rule out the possibility of a direct involvement of water molecules in the reaction center, although active site-solvent interaction turns out to be relevant in the energetics of the reaction. Essential dynamics analysis clearly shows that the Cpd0 product exists in two almost degenerate configurations, P₁ and P₂, basically differing in the His42 position.

Our results indicate that the title reaction evolves through an exothermic process accompanied by a relevant entropy increase; in particular, the largest contribution to the internal energy stabilization of 40 kJ/mol comes from the initial stage where the proton transfer occurs in a mechanically hindered local configuration. Alternatively, the protein-solvent relaxation steps, following the vertical proton transfer, are associated with entropy increase.

Finally, the present study shows that even in an apparently simple reaction, as the proton-transfer considered here, a proper, extended sampling of the atomic-molecular environment fluctuations and relaxations is essential to describe in a realistic manner both the QC-environment interaction and the reaction thermodynamics.

Similar information on the actual kinetics of the same reaction, currently under study in our laboratories, will plausibly require the same atomistic and statistical treatment of the entire system.

Acknowledgment. Work supported by Italian Consiglio Nazionale delle Ricerche (CNR, curiosity driven project, number 677). All of the calculations were performed at CASPUR using HP ProLiant DL585 cluster. We thank Pietro Vidossich for bringing to our attention his recent paper on this topic.

Appendix

Let us consider a portion of the simulated system, called quantum center (QC) undergoing a transition along a semi-classical (internal) coordinate hereafter termed as reaction coordinate (η). As already shown in our previous studies (see ref 18), the free energy associated with such a transition, within certain approximations, can be obtained by

$$\Delta A_{\eta_a \rightarrow \eta_b} = -k_B T \ln \langle \exp[-\beta(\epsilon_{\eta_b} - \epsilon_{\eta_a})] \rangle_{\eta_a} \quad (\text{I})$$

in which ϵ_{η_a} and ϵ_{η_b} represent the QC perturbed electronic ground-state energies evaluated at the η_a and η_b generic positions along the reaction coordinate (e.g., reactant and product) and averaging in the η_a ensemble (e.g., reactant). We can rewrite eq I as

$$\Delta A_{\eta_a \rightarrow \eta_b} = -k_B T \ln \frac{\int \exp(-\beta U'_{\eta_b}) d\mathbf{x}}{\int \exp(-\beta U'_{\eta_a}) d\mathbf{x}} \quad (\text{II})$$

where U' is the system potential energy (excess energy, see for example D'Abramo, M.; D'Alessandro, M.; Amadei, A. *J. Chem. Phys.* **2004**, *120*, 5526) and we considered the mass tensor of the system as essentially coordinate-independent, at least in the accessed range, hence removed from eq II.

By basic thermodynamics, we can express the internal energy change for the same process as

$$\Delta U_{\eta_a \rightarrow \eta_b} = \frac{\partial}{\partial \beta} (\beta \Delta A_{\eta_a \rightarrow \eta_b}) = \frac{\int U'_{\eta_b} \exp(-\beta U'_{\eta_b}) d\mathbf{x}}{\int \exp(-\beta U'_{\eta_b}) d\mathbf{x}} - \frac{\int U'_{\eta_a} \exp(-\beta U'_{\eta_a}) d\mathbf{x}}{\int \exp(-\beta U'_{\eta_a}) d\mathbf{x}} \quad (\text{III})$$

and hence

$$\Delta U_{\eta_a \rightarrow \eta_b} = \frac{\int U'_{\eta_b} \exp(-\beta U'_{\eta_b}) \exp(-\beta U'_{\eta_a}) \exp(\beta U'_{\eta_a}) d\mathbf{x}}{\int \exp(-\beta U'_{\eta_b}) \exp(-\beta U'_{\eta_a}) \exp(\beta U'_{\eta_a}) d\mathbf{x}} - \frac{\int \exp(-\beta U'_{\eta_a}) d\mathbf{x}}{\int \exp(-\beta U'_{\eta_a}) d\mathbf{x}} \langle U'_{\eta_a} \rangle_{\eta_a} \quad (\text{IV})$$

where

$$\langle U'_{\eta_a} \rangle_{\eta_a} = \frac{\int U'_{\eta_a} \exp(-\beta U'_{\eta_a}) d\mathbf{x}}{\int \exp(-\beta U'_{\eta_a}) d\mathbf{x}}$$

Within the approximations used in eq I, we have $U'_{\eta_b} - U'_{\eta_a} \cong \epsilon_{\eta_b} - \epsilon_{\eta_a} = \Delta\epsilon$ and hence

$$\Delta U_{\eta_a \rightarrow \eta_b} \cong \frac{\int \Delta\epsilon \exp(-\beta U'_{\eta_a}) \exp(-\beta \Delta\epsilon) d\mathbf{x}}{\int \exp(-\beta U'_{\eta_a}) d\mathbf{x} \langle \exp(-\beta \Delta\epsilon) \rangle_{\eta_a}} + \frac{\int U'_{\eta_a} \exp(-\beta U'_{\eta_a}) \exp(-\beta \Delta\epsilon) d\mathbf{x}}{\int \exp(-\beta U'_{\eta_a}) d\mathbf{x} \langle \exp(-\beta \Delta\epsilon) \rangle_{\eta_a}} - \langle U'_{\eta_a} \rangle_{\eta_a} \quad (\text{V})$$

where we used $U'_{\eta_b} = \Delta\epsilon + U'_{\eta_a}$. By multiplying and dividing, in eq V, $\langle U'_{\eta_a} \rangle_{\eta_a}$ by $\langle \exp(-\beta \Delta\epsilon) \rangle_{\eta_a} = \exp(-\beta \Delta A_{\eta_a \rightarrow \eta_b})$, we obtain

$$\Delta U_{\eta_a \rightarrow \eta_b} \cong \frac{\langle \Delta\epsilon \exp(-\beta \Delta\epsilon) \rangle_{\eta_a}}{\exp(-\beta \Delta A_{\eta_a \rightarrow \eta_b})} + \frac{\langle U'_{\eta_a} \exp(-\beta \Delta\epsilon) \rangle_{\eta_a}}{\exp(-\beta \Delta A_{\eta_a \rightarrow \eta_b})} - \frac{\int \exp(-\beta \Delta A_{\eta_a \rightarrow \eta_b}) \exp(-\beta U'_{\eta_a}) U'_{\eta_a} d\mathbf{x}}{\exp(-\beta \Delta A_{\eta_a \rightarrow \eta_b}) \int \exp(-\beta U'_{\eta_a}) d\mathbf{x}} \quad (\text{VI})$$

which can be rewritten as

$$\Delta U_{\eta_a \rightarrow \eta_b} \cong \frac{\langle \Delta\epsilon \exp(-\beta \Delta\epsilon) \rangle_{\eta_a}}{\exp(-\beta \Delta A_{\eta_a \rightarrow \eta_b})} + \frac{\langle (U'_{\eta_a} - \langle U'_{\eta_a} \rangle_{\eta_a}) (\exp(-\beta \Delta\epsilon) - \exp(-\beta \Delta A_{\eta_a \rightarrow \eta_b})) \rangle_{\eta_a}}{\exp(-\beta \Delta A_{\eta_a \rightarrow \eta_b})} \quad (\text{VII})$$

Finally, given the large size of the simulation box compared to QC and hence the system (overall) potential energy involves many degrees of freedom essentially independent of the QC electronic state, we may at first approximation consider

$$\frac{\langle (U'_{\eta_a} - \langle U'_{\eta_a} \rangle_{\eta_a}) (\exp(-\beta \Delta\epsilon) - \exp(-\beta \Delta A_{\eta_a \rightarrow \eta_b})) \rangle_{\eta_a}}{\exp(-\beta \Delta A_{\eta_a \rightarrow \eta_b})} \approx 0$$

hence providing

$$\Delta U_{\eta_a \rightarrow \eta_b} \approx \frac{\langle \Delta \epsilon \exp(-\beta \Delta \epsilon) \rangle_{\eta_a}}{\exp(-\beta \Delta A_{\eta_a \rightarrow \eta_b})} = \langle \Delta \epsilon \exp[-\beta(\Delta \epsilon - \Delta A_{\eta_a \rightarrow \eta_b})] \rangle_{\eta_a} \quad (\text{VIII})$$

which was used in the present paper.

References and Notes

- (1) Poulos, T. L.; Kraut, J. *J. Biol. Chem.* **1980**, *255*, 8199–8205.
- (2) Gajhede, M.; Schuller, D. J.; Henriksen, A.; Smith, A. T. *Nat. Struct. Biol.* **1997**, *4*, 1032–1038.
- (3) Baek, H. K.; Van Wart, H. E. *Biochemistry* **1989**, *28*, 5714–5719.
- (4) Gajhede, M. *Biochem. Soc. Trans.* **2001**, *29*, 91–152.
- (5) Douzou P. In *Oxidases and Related Redox Systems*; King, T. E., Mason, H. S., Morrison, M., Eds.; University Park Press: Baltimore, MD, 1973; Vol. I.
- (6) See for example: Denisov, I. G.; Makris, T. M.; Sligar, S. G. *J. Biol. Chem.* **2002**, *277*, 42706–42710.
- (7) Baek, H. K.; Van Wart, H. E. *J. Am. Chem. Soc.* **1992**, *114*, 718–725.
- (8) Rodriguez-Lopez, J. N.; Gilabert, M. A.; Tudela, J.; Thorneley, R. N. F.; Garcia-Canovas, F. *Biochemistry* **2000**, *39*, 13201–13209.
- (9) Jones, P.; Dunford, H. B. *J. Inorg. Biochem.* **2005**, *99*, 2292–2298.
- (10) Loew, G. H.; Dupuis, M. *J. Am. Chem. Soc.* **1996**, *118*, 10584–10587.
- (11) Woon, D. E.; Loew, G. H. *J. Phys. Chem. A* **1998**, *102*, 10380–10384.
- (12) Wirstam, M.; Blomberg, M. R. A.; Siegbahn, P. E. M. *J. Am. Chem. Soc.* **1999**, *121*, 10178–10185.
- (13) Zazza, C.; Aschi, M.; Palma, A. *Chem. Phys. Lett.* **2006**, *428*, 152–156.
- (14) (a) Derat, E.; Shaik, S. *J. Phys. Chem. B* **2006**, *110*, 10526–10533. (b) Derat, E.; Shaik, S.; Rovira, C.; Vidossich, P.; Alfonso-Prieto, M. *J. Am. Chem. Soc.* **2007**, *129*, 6346–6347.
- (15) Pu, J.; Gao, J.; Truhlar, D. *Chem. Rev.* **2006**, *106*, 3140–3169 and references therein.
- (16) Benkovic, S. J.; Hammes-Schiffer, S. *Science* **2003**, *301*, 1196–1202.
- (17) Aschi, M.; Di Nola, A.; Spezia, R.; Amadei, A. *Chem. Phys. Lett.* **2001**, *344*, 374–380.
- (18) Amadei, A.; D'Alessandro, M.; Aschi, M. *J. Phys. Chem. B* **2004**, *108*, 16250–16254.
- (19) Amadei, A.; D'Abramo, M.; Daidone, I.; D'Alessandro, M.; Di Nola, A.; Aschi, M. *Theor. Chem. Acc.* **2007**, *117*, 637–647.
- (20) Amadei, A.; D'Alessandro, M.; Paci, M.; Di Nola, A.; Aschi, M. *J. Phys. Chem. B* **2006**, *110*, 7538–7544.
- (21) Aschi, M.; D'Abramo, M.; Ramondo, F.; Daidone, I.; D'Alessandro, M.; Di Nola, A.; Amadei, A. *J. Phys. Org. Chem.* **2006**, *19*, 1650–1660.
- (22) D'Alessandro, M.; Aschi, M.; Paci, M.; Di Nola, A.; Amadei, A. *J. Phys. Chem. B* **2004**, *108*, 16255–16260.
- (23) Laberge, M.; Huang, Q.; Schweitzer-Stenner, R.; Fidy, J. *Biophys. J.* **2003**, *84*, 2542–2552.
- (24) Berendsen, H. J. C.; Postma, J. P. M.; van Gunsteren, W. F. In *Intermolecular Forces*; Pullman, B., Ed.; D. Reidel Publishing Company: Dordrecht, 1981; pp 331–342.
- (25) Amadei, A.; Chillemi, G.; Ceruso, M.; Grottesi, A.; Di Nola, A. *J. Chem. Phys.* **2000**, *112*, 9–23.
- (26) Berendsen, H. J. C.; Postma, J. P. M.; van Gunsteren, W. F.; A. Di Nola, A. *J. Chem. Phys.* **1994**, *81*, 3684–3690.
- (27) Hess, B.; Bekker, H.; Berendsen, H. J. C.; Frajje, J. G. E. M. *J. Comput. Chem.* **1997**, *18*, 1463–1472.
- (28) Darden, T. A.; York, D. M.; Pedersen, L. G. *J. Chem. Phys.* **1993**, *98*, 10089–10092.
- (29) van Gunsteren, W. F.; Billeter, S. R.; Eising, A. A.; Hunenberger, P. H.; Kruger, P.; Mark, A. E.; Scott, V. R. P.; Tirion, I. G. *Biomolecular Simulation: The GROMOS96 Manual and User Guide*; vdf Hochschulverlag AG an der ETH Zurich: Zurich, 1996.
- (30) Breneman, C. M.; Wiberg, K. B. *J. Comput. Chem.* **1990**, *11*, 361–367.
- (31) Parr, R. G.; Yang, W. *Density Functional Theory of Atoms and Molecules*; Oxford University Press, New York, 1989.
- (32) Hay, P. J.; Wadt, W. R. *J. Chem. Phys.* **1985**, *82*, 299–310.
- (33) Krishnan, R.; Binkley, J. S.; Seeger, R.; Pople, J. A. *J. Chem. Phys.* **1980**, *72*, 650–654.
- (34) Amadei, A.; Linssen, A. B. M.; Berendsen, H. J. C. *Proteins: Struct., Funct., Genet.* **1993**, *17*, 412–425.
- (35) Lindhal, E.; Hess, B.; Van der Spoel, D. *J. Mol. Model.* **2001**, *7*, 306–317.
- (36) (a) Aschi, M.; Zazza, C.; Spezia, R.; Bossa, C.; Di Nola, A.; Paci, M.; Amadei, A. *J. Comput. Chem.* **2004**, *7*, 974–984. (b) Spezia, R.; Aschi, M.; Di Nola, A.; Di Valentin, M.; Carbonera, D.; Amadei, A. *Biophys. J.* **2003**, *84*, 2805–2813. (c) Zazza, C.; Amadei, A.; Sanna, N.; Grandi, A.; Chillemi, G.; Di Nola, A.; D'Abramo, M.; Aschi, M. *Phys. Chem. Chem. Phys.* **2006**, *8*, 1385–1393.
- (37) Frisch, M. J.; Trucks, G. W.; Schlegel, H. B.; Scuseria, G. E.; Robb, M. A.; Cheeseman, J. R.; Montgomery, J. A., Jr.; Vreven, T.; Kudin, K. N.; Burant, J. C.; Millam, J. M.; Iyengar, S. S.; Tomasi, J.; Barone, V.; Mennucci, B.; Cossi, M.; Scalmani, G.; Rega, N.; Petersson, G. A.; Nakatsuji, H.; Hada, M.; Ehara, M.; Toyota, K.; Fukuda, R.; Hasegawa, J.; Ishida, M.; Nakajima, T.; Honda, Y.; Kitao, O.; Nakai, H.; Klene, M.; Li, X.; Knox, J. E.; Hratchian, H. P.; Cross, J. B.; Bakken, V.; Adamo, C.; Jaramillo, J.; Gomperts, R.; Stratmann, R. E.; Yazyev, O.; Austin, A. J.; Cammi, R.; Pomelli, C.; Ochterski, J. W.; Ayala, P. Y.; Morokuma, K.; Voth, G. A.; Salvador, P.; Dannenberg, J. J.; Zakrzewski, V. G.; Dapprich, S.; Daniels, A. D.; Strain, M. C.; Farkas, O.; Malick, D. K.; Rabuck, A. D.; Raghavachari, K.; Foresman, J. B.; Ortiz, J. V.; Cui, Q.; Baboul, A. G.; Clifford, S.; Cioslowski, J.; Stefanov, B. B.; Liu, G.; Liashenko, A.; Piskorz, P.; Komaromi, I.; Martin, R. L.; Fox, D. J.; Keith, T.; Al-Laham, M. A.; Peng, C. Y.; Nanayakkara, A.; Challacombe, M.; Gill, P. M. W.; Johnson, B.; Chen, W.; Wong, M. W.; Gonzalez, C.; Pople, J. A. *Gaussian 03*, revision C.02; Gaussian, Inc.: Wallingford, CT, 2004.
- (38) Mogharrab, N.; Ghourchian, H.; Amininasab, M. *Biophys. J.* **2007**, *92*, 1192–1203.
- (39) Rodriguez-Lopez, J. N.; Smith, A. T.; Thorneley, R. N. F. *J. Biol. Chem.* **1996**, *271*, 4023–4030.
- (40) The procedure is described, for example, in Amadei, A.; D'Abramo, M.; Di Nola, A.; Arcadi, A.; Cerichelli, G.; Aschi, M. *Chem. Phys. Lett.* **2007**, *434*, 194–199.